Long-lived charge separation following pump-wavelength–dependent ultrafast charge transfer in graphene/WS_2 heterostructures

Fu, Shuai; du Fossé, Indy; Jia, Xiaoyu; Xu, Jingyin; Yu, Xiaoqing; Zhang, Heng; Zheng, Wenhao; Krasel, Sven; Houtepen, Arjan J.; More Authors

DOI
10.1126/sciadv.abd9061

Publication date
2021

Document Version
Final published version

Published in
Science Advances

MATERIALS SCIENCE

Long-lived charge separation following pump-wavelength–dependent ultrafast charge transfer in graphene/WS_2 heterostructures

Shuai Fu[1], Indy du Fossé[2], Xiaoyu Jia[1], Jingyin Xu[1,3], Xiaoqing Yu[1], Heng Zhang[1], Wenhao Zheng[1], Sven Krasel[1], Zongping Chen[4], Zhiming M. Wang[3], Klaas-Jan Tielrooij[5], Mischa Bonn[1], Arjan J. Houtepen[2], Hai I. Wang[1]*

Van der Waals heterostructures consisting of graphene and transition metal dichalcogenides have shown great promise for optoelectronic applications. However, an in-depth understanding of the critical processes for device operation, namely, interfacial charge transfer (CT) and recombination, has so far remained elusive. Here, we investigate these processes in graphene-WS_2 heterostructures by complementarily probing the ultrafast terahertz photoconductivity in graphene and the transient absorption dynamics in WS_2 following photoexcitation. We observe that separated charges in the heterostructure following CT live extremely long: beyond 1 ns, in contrast to ~1 ps charge separation reported in previous studies. This leads to efficient photogating of graphene. Furthermore, for the CT process across graphene-WS_2 interfaces, we find that it occurs via photo-thermionic emission for sub-A-exciton excitations and direct hole transfer from WS_2 to the valence band of graphene for above-A-exciton excitations. These findings provide insights to further optimize the performance of optoelectronic devices, in particular photodetection.

INTRODUCTION

Atomically thin layers, including graphene and monolayer transition metal dichalcogenides (TMDCs), represent a fascinating material class for electronic and optoelectronic applications. As a bond-free strategy, stacking these two-dimensional (2D) layers allows the production of artificial van der Waals (vdW) heterostructures, which offers the prospect of discovering new synergetic electronic, optical, and magnetic phenomena (*1*–*4*). Thanks to the development of precise control over composition, layer numbers, stacking angles, and sequences of the atomic layers, the past decade has witnessed the blossoming of novel concepts and high-performance devices based on vdW heterostructures (*5*–*7*). One notable example is that the integration of graphene and monolayer TMDCs enables sensitive photodetectors with high photoresponsivity (R_{ph}) up to 10^7 A W^{-1} at room temperature (*8*), comparable to state-of-the-art photodetectors based on graphene–quantum dot (g-QD) hybrid system with R_{ph} up to 10^8 A W^{-1} (*9*).

There has been a great and successful effort to increase the efficiency of graphene-TMDC (g-TMDC) photodetectors, but the understanding of the fundamental photophysics of these devices has remained elusive. For instance, recent spectroscopic studies (*10*–*12*) have reported a very fast (~1 ps) charge recombination (via back electron transfer process) at g-WS_2 interfaces. Such a short charge separation lifetime seems in contradiction to the large R_{ph} reported in the photodetectors based on g-TMDCs heterostructures. For other g-based hybrid photodetectors, e.g., g-PbS QD photodetectors (*9*), an extremely long interfacial charge separation time (~20 ms) has been attributed to carrier trapping in the QDs. The long-lived interfacial charge separation establishes an electric field at vdW interfaces, leading to photoconductive gain and, thus, a high R_{ph} in the photodetectors (the so-called "photogating effect," in analogy to field-effect gating). As the photoconductive gain (G) is linearly proportional to the charge separation lifetime (τ_{CS}) (*13*), it remains unclear how efficient photodetectors can be realized in g-TMDC heterostructures (*5*, *14*, *15*) with a reported τ_{CS} of ~1 ps.

Along with the controversy on the charge separation lifetime, the second puzzle regarding the (interfacial) charge carrier dynamics in g-TMDC heterostructures lies in the efficiency and underlying mechanisms of charge transfer (CT) processes. Immediately following photoexcitation of bare graphene, the photogenerated, nonthermalized hot carriers can efficiently transfer their excess energy to other charge carriers within tens of femtoseconds via carrier-carrier scattering (*16*–*19*). This thermalization process leads to the formation of thermalized hot carriers with a well-defined electron temperature (T_e) following the Fermi-Dirac distribution (*20*, *21*). The thermalized hot carriers undergo a cooling process within a few picoseconds via electron-phonon scattering (*22*–*26*). In g-TMDC vdW heterostructures, TMDCs can serve as transport channels to harvest hot carriers (in principle, for both nonthermalized and thermalized hot carriers) from graphene before the cooling process takes place. Pioneering device works (*27*, *28*) have shown that hot electron transfer (HET) contributes to the photocurrent generation at g-based vdW interfaces, which has been further confirmed by ultrafast spectroscopic studies (*10*–*12*). However, the mechanism of HET across vdW interfaces, and in particular whether HET occurs before or after thermalization, remains highly debated. For instance, in the device work by Massicotte *et al.* (*27*), the photocurrent generation in a g-WSe_2–g vdW heterostructure following below-WSe_2-bandgap excitation is attributed to photo-thermionic emission, in

[1]Max Planck Institute for Polymer Research, Ackermannweg 10, D-55128 Mainz, Germany. [2]Optoelectronic Materials Section, Faculty of Applied Sciences, Delft University of Technology, Van der Maasweg 9, 2629 HZ Delft, Netherlands. [3]Institute of Fundamental and Frontier Sciences, University of Electronic Science and Technology of China, Chengdu 610054, P. R. China. [4]School of Materials Science and Engineering, Zhejiang University, Zheda Road 38, Hangzhou 310027, China. [5]Catalan Institute of Nanoscience and Nanotechnology (ICN2), BIST and CSIC, Campus UAB, Bellaterra, 08193 Barcelona, Spain.
*Corresponding author. Email: wanghai@mpip-mainz.mpg.de

which thermalized hot electrons with energy above the interfacial energy barrier can be injected into WSe_2 (with a quantum yield of ~1%). In sharp contrast, Chen *et al.* (*10*) recently proposed that HET at g-WS_2 interfaces competes with the thermalization in graphene and shows an extremely high quantum yield (~ 50%). Furthermore, Yuan *et al.* (*11*) suggested an alternative model for HET at g-WS_2 interfaces, in which a direct excitation from graphene to WS_2 can take place via CT states due to strong interfacial electronic coupling. It is apparent that further studies on HET across g-TMDCs interfaces are required to solve this debate. Furthermore, while the contribution of hot electrons to CT has been recognized, it remains unclear if the "cold" electrons, e.g., the valance band electrons in graphene, are involved in interfacial CT at g-TMDC interfaces.

Here, aiming to provide a comprehensive understanding of the interfacial carrier dynamics in g-WS_2 vdW heterostructures, we measure complementarily the ultrafast photoconductivity dynamics in graphene by terahertz (THz) spectroscopy (Fig. 1A) and the excited-state dynamics in TMDCs by transient absorption (TA) spectroscopy (Fig. 1B) following photoexcitation with a wide range of photon energies from 0.7 to 3.1 eV. The unique combination of THz and TA spectroscopies enables us to track the charge carrier dynamics in both the donor and acceptor independently and to identify and quantify the trapping process (if active) at the interfaces. We find that the charge separation lifetime following ultrafast CT is remarkably long-lived, beyond 1 ns (limited by the scan range of the setup). This observation is in sharp contrast to the short-lived excited-state dynamics (~1 ps) in WS_2 observed by TA, both in this study and in previous works (*10*, *11*). We rationalize the discrepancy between the carrier lifetime in the electron donor (graphene) and the acceptor (WS_2) by the presence of trap states at g-WS_2 interfaces. These trap states can effectively capture the electrons from the excited states of WS_2 within 1 ps (corresponding to the fast decay in TA dynamics) and further store them for over 1 ns (corresponding to the long-lived photoconductivity in graphene by THz study) before recombining with the holes in graphene. This leads to a long-lived photogating effect in graphene. On the other hand, for the forward CT process from graphene to WS_2, we unveil two distinctively different CT regimes when exciting the heterostructure below (0.7 to 2 eV) or above the A-exciton resonance (2 to 3.1 eV) of monolayer WS_2. Exciting below the WS_2 A-exciton transition, we find that a relatively inefficient (~1%) HET via photo-thermionic emission governs the CT process, in which thermalized hot electrons in graphene are emitted over the energy barrier and transferred into WS_2 (Fig. 1C). In the second regime where the photoexcitation is above the A-exciton resonance of WS_2, we report a more efficient (up to ~5%) direct hole transfer (DHT) mechanism, which involves the photogenerated holes in the valence band of WS_2 and electrons in the valence band of graphene (Fig. 1D).

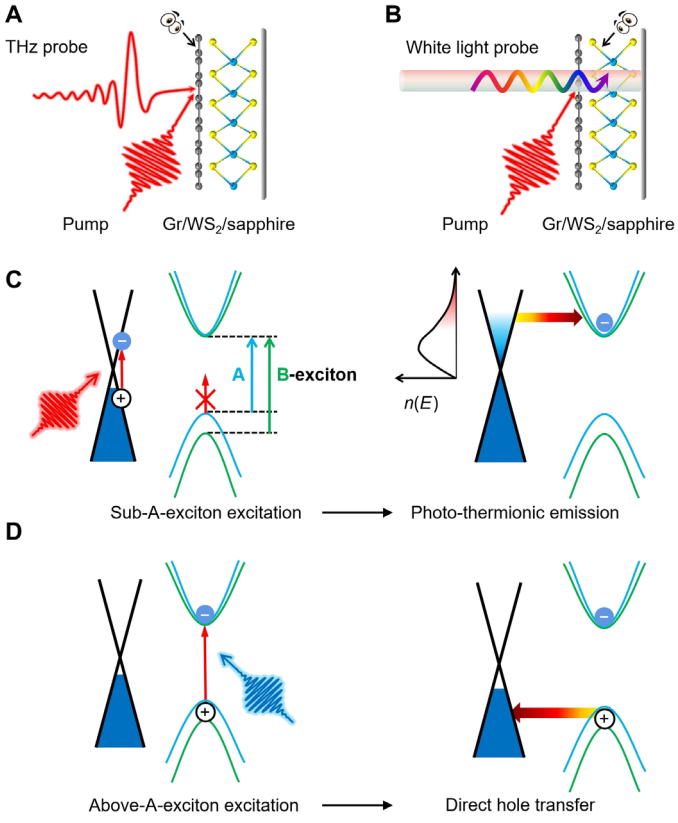

Fig. 1. Investigation of the nonequilibrium hot carrier dynamics at g-WS_2 interfaces. (**A**) Schematic of using ultrafast THz spectroscopy to measure the photoconductivity of graphene following photoexcitation. (**B**) Scheme of ultrafast TA spectroscopy to measure the excited-state dynamics of WS_2 following photoexcitation. (**C**) Illustration of interfacial band alignment and photo-thermionic emission for thermalized hot electrons following sub-A-exciton excitation, in which thermalized hot electrons in graphene can be emitted over the energy barrier and transferred into the excited states of WS_2. A- and B-exciton transitions in WS_2, originating from the spin-split valence bands at the K point of the Brillouin zone, are marked. (**D**) Schematic of direct hole transfer (DHT) at g-WS_2 interfaces following above-A-exciton excitation, in which the photogenerated holes in the valance band of WS_2 recombine with valence band electrons in graphene.

RESULTS

The g-WS_2 heterostructure used in this study was obtained commercially (from SixCarbon Technology, Shenzhen). It is produced by transferring a chemical vapor–deposited (CVD) graphene monolayer onto a CVD WS_2 monolayer, grown on a sapphire substrate (schematically depicted in fig. S1A). As both layers are multicrystalline with a typical domain size of several micrometers, the dynamics that we are probing is an average response of the heterostructure with mixed twisting angles (given that the probe beam has a diameter of ~0.5 to 1 mm for THz measurements and ~0.1 mm for TA measurements). In an independent electrical four-point probe measurement of the resistivity of graphene (produced by the same method) at varied gating potentials, we find that the graphene in the heterostructure is initially p-doped, in line with previous reports (*10*) for the same system. Before studying the ultrafast carrier dynamics, we have characterized the static optical and electronic properties of the heterostructure using ultraviolet-visible (UV-vis) absorption and Raman spectroscopy. We observe two exciton resonances at 2.0 and 2.4 eV in the absorption spectra (fig. S1B), corresponding to the A- and B-exciton transitions from the spin-split valence bands at the K point of the Brillouin zone in monolayer WS_2 (*29*–*31*), respectively (see also the simplified band structure of WS_2 in Fig. 1, C and D). The featureless constant absorption (~2.3%) in the near-infrared range originates from the absorption of monolayer graphene (*32*, *33*). Raman studies shown in fig. S1 (C and D) further confirm that both the graphene and WS_2 layer are monolayers in nature. On the basis of the G-band position in graphene, we can estimate the Fermi level

(E_F) in graphene to be ~0.11 eV (equivalent to a free carrier density N of 7.9×10^{11} cm^{-2}; see section S1) below the Dirac point (given the p-doped nature of graphene from electrical measurements). We have further verified E_F in graphene using THz-time domain spectroscopy (THz-TDS; see section S2). In short, in the THz-TDS measurements, we record the THz electric field transmitted through the WS_2/sapphire substrate configurations in the time domain, with and without graphene on the top, i.e., $E(t)$ (for graphene/WS_2/sapphire) and $E_0(t)$ (for WS_2/sapphire), respectively. The obtained time-dependent THz fields are further converted into the frequency domain by Fourier transform as $E(\omega)$ and $E_0(\omega)$. The THz absorption, because of the presence of free charges in graphene, can be well described by the Drude model, which provides microscopic transport properties in graphene, including the charge carrier density (or Fermi level). On the basis of THz-TDS results, we estimate the E_F in graphene to be 0.1 eV versus the Dirac point [see fig. S1 (E and F) and the associated discussions in section S2], in excellent agreement with our Raman measurements.

Ultrafast interfacial CT and long-lived charge separation in g-WS_2 vdW heterostructures probed by THz spectroscopy

We investigate the dynamics of photogenerated charge carriers in the g-WS_2 system by optical pump-THz probe (OPTP) spectroscopy. In a typical OPTP measurement, as shown in Fig. 1A, an optical pump with ~50-fs duration selectively excites either only the graphene layer (sub-A-exciton transition in WS_2, $h\nu < 2$ eV) or both layers in the heterostructure at a fixed sample spot ($h\nu > 2$ eV). The pump-induced photoconductivity ($\Delta\sigma$) is probed by a THz pulse by monitoring the change in the transmitted electrical field ($\Delta E = E_{pump} - E_0$) following the optical pump as a function of pump-probe delay. The measurement is based on the principle that $-\Delta E$ is proportional to $\Delta\sigma$ (*34*).

As control measurements, we first investigate the carrier dynamics of the individual monolayer WS_2 and graphene upon 1.55-eV excitation. As the excitation energy is still below the A-exciton resonance of monolayer WS_2, we observe no photoconductivity (Fig. 2A, blue line) for monolayer WS_2, as expected. On the other hand, the same excitation energy for graphene yields a transient reduction in the conductivity, i.e., negative photoconductivity (Fig. 2A, gray circle points). The negative photoconductivity in doped graphene has been widely reported previously (*19*, *35*–*40*) and can be briefly understood as follows: Following optical excitation and the rapid thermalization in the doped graphene, the increased carrier temperature leads to a reduced screening of the long-range Coulomb scattering and, thus, reduced conductivity (*38*). Within a few picoseconds, these thermalized hot carriers cool down to the initial thermal equilibrium via electron-phonon scattering.

For g-WS_2 heterostructures, one could, in the first instance, expect the photoconductivity upon 1.55-eV excitation to be a superposition of that of individual monolayer graphene and WS_2, i.e., exhibiting an overall negative photoconductivity with sub–10 ps lifetime. However, we observe distinctively different dynamics for the heterostructure upon 1.55-eV excitation (Fig. 2A, red line): After the short-lived negative photoconductivity, the photoconductivity turns positive within 10 ps, followed by a remarkably long-lived positive photoconductivity with a lifetime extending 1 ns (without decay in 1 ns for some cases, see statistics for the measurements of seven different sample areas in section S3). While the short-lived negative contribution can be attributed to the hot state of the graphene electronic system, the long-lived positive contribution appears only in the heterostructure. We assign this positive photoconductivity to an interfacial charge-transfer process across g-WS_2 interfaces (which is supported by TA measurements in Fig. 2D below). Furthermore, we find that the lifetime of the long-lived photoconductivity does not depend on pump photon energy (see fig. S2B). We attribute this positive, long-lived photoconductivity and its independence on excitation photon energy to photogating effect in the vdW heterostructure: Following photoexcitation, electrons are first transferred from graphene to WS_2 on a sub-picosecond time scale and subsequently get trapped at interfacial states where they remain for over 1 ns. For the initially p-doped graphene layer, extracting electrons from graphene results in a shift of Fermi level further away from the Dirac point, and thus an increase of conductivity in graphene. To confirm such a Fermi-level downshift following excitation and electron transfer from graphene to WS_2, we analyze the frequency dependence of the complex THz photoconductivity by THz-TDS (see details in section S2). The pump-probe delay (τ) is chosen at ~100 ps to avoid the intrinsic hot carrier state in graphene, which has a lifetime of ~10 ps. As shown in Fig. 2B, we find the frequency-resolved THz photoconductivity can be well fitted with the Drude model, indicating that free carriers dominate the THz photoconductivity, with a scattering time of 69 fs (see details in section S2). On the basis of the fit, E_F of graphene at $\tau = 100$ ps following 1.55-eV excitation is 0.14 eV below the Dirac point (equivalent to $N = 1.1 \times 10^{12}$ cm^{-2}), indicating a 30- to 40-meV downshift of E_F in graphene following electron transfer from graphene to WS_2 (given the initial E_F of 0.1 to 0.11 eV).

CT dynamics and interfacial charge separation time probed by TA spectroscopy

To provide a direct spectroscopic signature of electron injection from graphene to WS_2, we have performed complementary measurements using TA spectroscopy. Along with providing direct evidence for CT across the heterostructures, using TA spectroscopy is further motivated by noticing a large discrepancy between the charge separation lifetime obtained by our THz results (beyond 1 ns) and previous TA results (reported to be ~1 ps). By probing the corresponding excited-state absorption changes with a pump-probe scheme, the charge occupation dynamics in WS_2 can be directly obtained with a subpicosecond time resolution. As shown in Fig. 2C, we observe no photobleaching (PB) signal when exciting the individual monolayer WS_2 with 1.55-eV pulses (below its A-exciton resonance), in line with our THz results (Fig. 2A, blue line). This result also indicates that the pump fluence used in this study is sufficiently low to avoid notable two-photon absorption in WS_2. A small, short-lived differential-like dynamic (with a lifetime of ~150 fs as shown in Fig. 2E) is noticed and may be attributed to the coherent artifact, predominantly as a result of the optical Stark effect, which has been widely reported previously (*41*). In contrast, for the g-WS_2 heterostructure, we observe two PB signals at both the A- and B-exciton resonances of monolayer WS_2 (2.0 and 2.4 eV, respectively) for the same excitation energy and similar pump fluence, as shown in Fig. 2D. Note that, for monolayer WS_2, A- and B-exciton resonances originate from two spin-split valence bands at the K point (*29*, *30*). For the conduction bands, the spin splitting is usually small, resulting in quasi-degeneracy of the two spin splitting bands (see Fig. 1D). Thanks to this effect, the simultaneous occurrence of PB at both A- and B-exciton resonances provides additional evidence of the injection of (hot) electrons rather than holes from graphene to

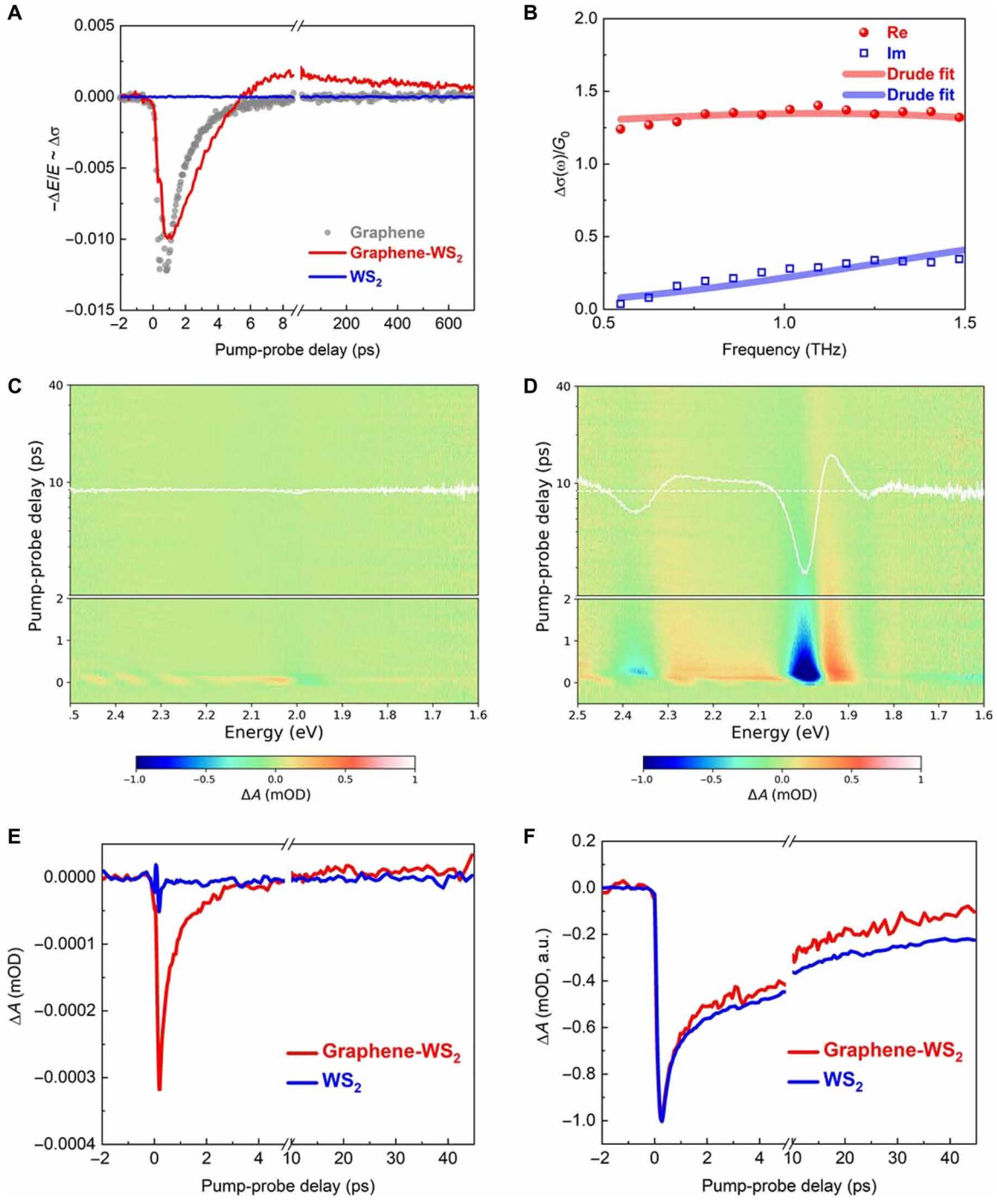

Fig. 2. Ultrafast interfacial CT and long-lived charge separation in graphene-WS_2 vdW heterostructures. (**A**) OPTP carrier dynamics for graphene (gray circle points), WS_2 (blue line), and the g-WS_2 heterostructure (red line). Samples are measured with 1.55-eV excitation under dry N_2 purging conditions. The absorbed photon densities are 3.8×10^{12}, 3.7×10^{12}, and 0.8×10^{12} cm^{-2} for WS_2, g-WS_2 heterostructure, and graphene, respectively. (**B**) Complex photoconductivity for g-WS_2 heterostructure at a pump-probe delay of ~100 ps under 1.55-eV excitation with an absorbed photon density of 2.6×10^{13} cm^{-2}. Red and blue lines represent the Drude fit for the real and imaginary part of the complex photoconductivity, respectively. We use the conductivity unit in quantum conductance $G_0 = 2e^2/h$; 2D TA color map for (**C**) monolayer WS_2 and (**D**) g-WS_2 heterostructure following 1.55-eV excitation with pump fluences of 670 and 620 μW, respectively. mOD, milli optical density. The white lines in (C) and (D) represent the spectral slices averaged between 0.5 and 1 ps. (**E**) TA carrier dynamics averaged over the A-exciton resonance (between 1.88 and 2.07 eV) for g-WS_2 heterostructure (red line) and monolayer WS_2 (blue line) following 1.55-eV excitation with a pump fluence of 670 and 620 μW, respectively. (**F**) TA carrier dynamics averaged over the A-exciton resonance (between 1.88 and 2.07 eV) for g-WS_2 heterostructure (red line) and monolayer WS_2 (blue line) following 3.10-eV excitation with pump fluences of 248 and 250 μW, respectively. a.u., arbitrary units.

WS_2 following sub-A-exciton excitation. If not, then one expects only PB at A-exciton resonance for the hole injection into WS_2.

We find that the injected electrons in the excited states in WS_2 decay within 1 ps as shown in Fig. 2E, in sharp contrast to over 1-ns charge separation lifetime in g-WS_2 heterostructures based on our THz results shown in Fig. 2A. Note that the short excited-state dynamics observed here is in line with previous TA measurements (*10*, *11*). In these studies, the ultrafast depopulation process was attributed to back electron transfer from WS_2 to graphene. Therefore, the large difference in the measured carrier lifetime in the donor (graphene) and the acceptor (WS_2) suggests a new recombination pathway.

Interfacial photogating effect in g-WS_2 heterostructure is supported by interfacial states

Here, we attribute the long-lived (over ~1 ns) photoconductivity in graphene (by THz spectroscopy) to an interfacial photogating mechanism mediated by interfacial states (e.g., defects) at g-WS_2 interfaces. In such a scheme, following photoexcitation, electrons in WS_2, either directly generated by excitation (with $h\nu > 2$ eV) or injected from graphene to the conduction band of WS_2 (for $h\nu < 2$ eV), are subsequently trapped (within ~1 ps) to long-lived interfacial states. The relatively long-lived trapped electrons can effectively gate graphene, leading to an efficient modification of the carrier density (thus the Fermi level) in graphene (observed by THz spectroscopy). Intriguingly, following the fast ~1-ps PB decay, the TA dynamics is dominated by a much longer-lived, spectral shift (with the differential-like feature; see the dynamics and the spectral slices in Fig. 2D). This feature can be understood by a transient electrical field–induced Stark effect, following ultrafast CT and trapping at the interface. Such spectral shift due to the local electrical field built at the interfaces has previously been reported in heterostructures consisting of semiconducting quantum dots (*42*).

Now, we briefly discuss the possible origin of the "interfacial" states for photogating effect. First, as the energies of these states lie between the conduction band of WS_2 and the Fermi level of graphene, it seems reasonable to assume that they originate from defect states present in the WS_2 layer or hybridized states at interfaces. To test this hypothesis and shed light on the nature of these states, we have studied and compared the TA dynamics of monolayer WS_2 and g-WS_2 heterostructure following 3.10-eV excitation. As shown in Fig. 2F, we observe very similar decay dynamics for both samples (especially for the fast initial decay). This result strongly suggests a universal recombination pathway at the first 1 to 2 ps, very likely due to trapping in the defect states in WS_2. Note that this assumption is in line with previous THz and TA dynamics reported in monolayer TMDCs, where the fast, ~1-ps decay is also assigned to charge trapping (*43*–*45*). In addition, a relatively slow process with >10-ps lifetime is also observed, which can be assigned to trap-assisted recombination following previous reports (*43*, *46*).

According to literature, we speculate that the defect states could originate from sulfur vacancies, which are ubiquitously present in CVD-WS_2. For instance, a recent report combining ab initio GW calculations and scanning tunneling spectroscopic studies has shown that sulfur vacancies in WS_2 can generate two types of unoccupied in-gap states, which are located ~0.5 and 0.7 eV below the conduction band of WS_2, respectively (*47*), with at least one of them lying between the Fermi level of graphene and the conduction band of monolayer WS_2. These empty defect states can serve as the "intermediate" trap sites, which can electrostatically gate the graphene layer. By quantifying the density of transferred charges (see the THz-TDS study in the next section), we can set a lower limit for the defect density in our sample of 3.2×10^{11} cm^{-2}, by assuming that the same amount of charges are trapped for the photogating process. This value is consistent with the values reported in the literature (*48*, *49*). Further studies using photo-electrochemical methods (*50*–*52*) to unveil the energetics and the nature of the involved defects at the g-WS_2 interfaces could shed light on this issue. By tuning the Fermi level in graphene via, e.g., ionic gating, we can intentionally fill the defects in WS_2 responsible for the photogating process. By monitoring the gate voltage–dependent recombination rates, one should be able to map out the density and energetics of the defect states.

CT rate and mechanism at g-WS_2 interfaces

Exploiting the long-lived photogating effect, we further investigate the mechanism underlying ultrafast CT at g-WS_2 vdW interfaces on early time scales. The positive photoconductivity originating from the photogating effect provides a direct measure to the number of electrons transferred across the interfaces. We estimate the energy barrier for CT to be ~0.8 eV, by taking into account the energy difference between WS_2 conduction band minimum (CBM) and the Fermi level in graphene, as well as corrections including the bandgap reduction in WS_2 due to dielectric screening of graphene (*53*), and shifts in energetics associated with CT (see details in section S4). We found that the estimated energy barrier for CT is in line with previous studies (*10*). Given this large barrier and the fact that only graphene is excited by 1.55-eV pump photons (thermalized or nonthermalized), hot carriers are necessarily involved in the interfacial CT process at g-WS_2 interfaces. For most spectroscopic studies up to now, the optical excitation is limited to either below (*10*, *11*) or only at the A-exciton resonance of TMDCs (*12*). To investigate whether and how the excitation energy or the initial charge configuration affects CT channels and mechanisms, we monitor the CT dynamics at various photoexcitation fluences and with a broad range of photon energies ($h\nu$) from 0.7 eV (which only excites graphene) to 3.1 eV (which excites both graphene and WS_2), across the A-exciton resonance (2 eV) of WS_2.

In Fig. 3A, we present typical fluence-dependent CT dynamics for g-WS_2 heterostructure following 1.38-eV excitation. The long-lived positive photoconductivity increases with increasing absorbed photon density. To qualitatively describe the CT efficiency under different excitation conditions, we extract the maximum positive photoconductivity [$\Delta\sigma_{max} \sim (-\Delta E/E)_{max}$] for different pump energies and fluences, as shown in Fig. 3B. For the pump photon energies and fluences used, we always observe positive long-lived photoconductivity. This indicates that, for all cases, CT involves electron injection from graphene to WS_2 (or equivalently, hole transfer from WS_2 to graphene). Intriguingly, for the lowest photoexcitation energy used in this study (0.7 eV), the excess energy ($E_{ex} = h\nu/2 - E_F$) in the photogenerated nonthermalized hot electrons is only ~0.45 eV, which is way below the energy barrier for CT at g-WS_2 interfaces (~0.8 eV). The fact that we nonetheless observe a positive photoconductivity indicates that CT takes place following thermalization via so-called photo-thermionic emission (*27*). This photo-thermionic emission scheme relies on very high electron temperatures in graphene reached for typical incident excitation powers. Sufficiently hot electrons in the valence band can be heated across the Dirac point into the conduction band. Following this interband heating process (*38*),

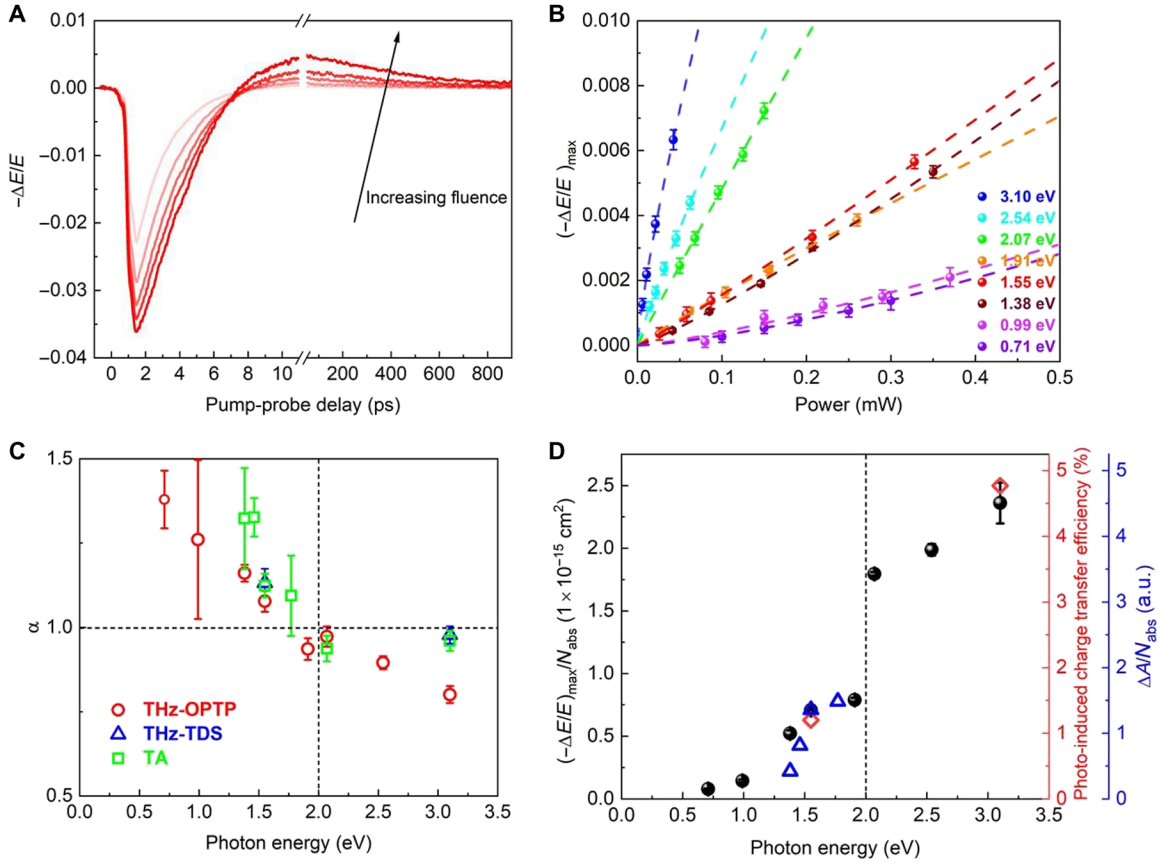

Fig. 3. CT efficiency and mechanism at graphene-WS_2 interfaces. (**A**) Fluence-dependent CT dynamics at g-WS_2 interfaces. Samples are measured using 1.38-eV excitation with a series of absorbed photon densities, from 6.6×10^{11} to 5.6×10^{12} cm^{-2}. (**B**) Summary of the fluence-dependent photoconductivity maximum of $-\Delta E/E$ [i.e., $(-\Delta E/E)_{max}$] for different photon excitation energies, from $h\nu = 0.71$ to 3.10 eV. The data are described by a simple power law, namely, $(-\Delta E/E)_{max} = A \cdot P^{\alpha}$ ($\alpha \geq 0$), as described in the main text. (**C**) Photon energy–dependent power index α obtained by THz-OPTP, THz-TDS, and TA methods. For above-A-exciton excitations, α is close to 1 for TA and THz-TDS, while it is smaller than 1 for OPTP. We attribute this discrepancy to the different physical quantities measured by the tools (transferred charge carrier density for TA and THz-OPTP versus photoconductivity for OPTP; see details in the Supplementary Materials). (**D**) Quantification of photon energy–dependent CT efficiency in the heterostructure. The black dots represent the "relative" CT efficiency estimated by THz-OPTP data (the left *Y* axis), while the red diamonds stand for the absolute CT efficiency estimated by THz-TDS data (the right red *Y* axis), and the blue triangles represent the relative CT efficiency estimated by TA data in the sub-A-exciton excitation regime (the right blue *Y* axis).

the thermalized hot electrons with sufficient energy over the energy barrier at g-WS_2 interfaces can be injected into WS_2. We calculate the electron temperature (T_e) in graphene as a function of incident fluence based on the photo-induced THz response of graphene (see details in section S5). As shown in fig. S3A, T_e can reach 1500 to 3000 K over our fluence range. Figure S3C shows the resultant hot electron distribution following the thermalization. A substantial fraction of thermalized hot electrons (~22.2% with T_e of 2700 K) reaches energies in excess of the conduction band in WS_2, in good agreement with our proposed photo-thermionic emission scheme. We conduct a similar analysis for thermalized hot holes in the valence band in graphene. We observe a much smaller fraction (~1.6% with T_e of 2700 K) of thermalized hot holes with energy above the energy barrier for hole injection than that of thermalized hot electrons in our system (see fig. S3D), because of the larger energy separation between the Fermi level in graphene and the valence band in WS_2 (~1.3 eV). This result can explain our experimental observation of the injection of thermalized hot electrons rather than holes from graphene to WS_2 in the study.

In principle, the photoconductivity caused by the photo-thermionic emission should exhibit a superlinear dependence on the pump fluence (*27*, *28*) (see also the simulation result shown in fig. S3E). We therefore describe the pump fluence–dependent maximum positive photoconductivity with P^{α} as shown in Fig. 3B, where P is the pump power, and α is the power index ($\alpha > 1$ for superlinear dependence). In Fig. 3C, we show the extracted values of $\alpha_{THz\text{-}OPTP}$ for different photon excitation energies. We find that $\alpha_{THz\text{-}OPTP}$ is bigger than 1 when the photon excitation energy is below the A-exciton resonance of WS_2. With increasing photon excitation energy, $\alpha_{THz\text{-}OPTP}$ gradually decreases and undergoes a transition around the A-exciton resonance of WS_2, from above 1 ($\alpha \sim 1.4$ at 0.7-eV excitation, superlinear) to slightly below 1 ($\alpha \sim 0.9$ for $h\nu > 2$ eV, sublinear). It is worth noting that in previous TA studies (*10*, *11*), a linear fluence dependence (i.e., $\alpha = 1$) of the signal was reported, following sub-A-exciton excitation. Therefore, to further verify our THz results, we have repeated the fluence-dependent measurements for the same sample using other complementary methods, including THz-TDS and TA spectroscopy (see details of our TA study in the

last section). The power indexes α obtained from these three methods are found to behave similarly, as shown in Fig. 3C (detailed analysis and discussions of the experimental data can be found in section S6). This result shows that the change in α is independent of the used spectroscopic tools.

We attribute this superlinear-to-sublinear pump fluence dependence of the CT dynamics to a transition between two distinct CT regimes: HET via photo-thermionic emission for sub-A-exciton excitation (see Fig. 1C) and DHT for above-A-exciton excitation. The DHT process involves the interfacial recombination of holes in the valence band of WS_2 with valence band electrons in graphene (see Fig. 1D). A slightly sublinear feature in our study can be understood as follows: With increasing fluence, many-body effects, for instance, exciton-exciton annihilation in TMDCs (*54*), can play a critical role in the charge carrier dynamics on the subpicosecond to picosecond time scale. These many-body effects can result in a decrease in the hole density in TMDCs, which reduces the CT efficiency at high fluence. Note that in the above-A-exciton excitation regime, hot electrons in graphene, despite having higher energy than those generated by sub-A-exciton excitation (for a given absorbed power), contribute little to CT. This is mainly due to the much weaker absorption in graphene in comparison to that in WS_2. On top of that, we discuss other CT pathways, including photo-thermionic emission and hole transfer from WS_2 to the photoexcited hot electrons in graphene in the above-A-exciton excitation regime (see the extended discussions in section S7) and argue that they cannot compete with the DHT process.

It is worth commenting that our results and the proposed microscopic model agree well with a recent study by time-resolved angle-resolved photoemission spectroscopy. In the study (*12*), an ultrafast (sub–200 fs) loss of the valence band electrons in graphene has been directly observed in the same heterostructure by resonantly exciting the A-exciton resonance of monolayer WS_2. Furthermore, for the photocurrent generation in g-based heterostructures (*21*, *22*), the photo-thermionic emission is proposed to govern the photocurrent generation for low photoexcitation energy, whereas direct interlayer tunneling becomes the dominant mechanism for high photoexcitation energy. Our results here are also in line with these macroscopic device results and further provide macroscopic mechanisms for the interfacial CT processes. Last, despite the clear difference in CT mechanisms between the two regimes discussed, we note that the resultant charge configurations at the interfaces are indistinguishable with electrons in the excited state of WS_2 and holes in the valence band of graphene.

To further confirm the proposed two CT regimes, we quantify their efficiency at different excitation energies. Here, we use two approaches to determine the interfacial CT efficiency based on THz-TDS and OPTP results: (i) we define the absolute CT efficiency as $\eta = N_{CT}(h\nu)/N_{abs}$, where $N_{CT}(h\nu)$ is the number of electrons injected from graphene to WS_2 at excitation energy $h\nu$, and N_{abs} represents the absorbed photon density in the donor, i.e., graphene for the photo-thermionic emission regime and WS_2 for the DHT regime. N_{CT} and N_{abs} are experimentally accessible by THz-TDS (see details in section S2) and absorption measurements (see details in section S1), respectively; (ii) on the basis of the OPTP results shown in Fig. 3B, we can directly compare the maximum positive photoconductivity at a fixed absorbed photon density (approximately 5×10^{12} cm^{-2}). At the pump-probe delay where the positive photoconductivity is maximum (~15 ps), charge carriers in our system reach quasi-equilibrium following ultrafast CT, so that the carrier mobility μ of graphene is nearly constant over time. As the photoconductivity Δσ is proportional to the products of μ and $N_{CT}(h\nu)$, $\Delta\sigma/N_{abs}$ at the maximum positive photoconductivity reflects the relative change in the CT efficiency under different photon excitation energies.

In Fig. 3D, we plot the CT efficiencies obtained by (i) THz-TDS (as right *Y* axis) and (ii) OPTP (as left *Y* axis) as a function of photon excitation energy. For 1.55- and 3.10-eV excitations, where both methods are applied, the CT efficiencies evaluated by these two methods agree perfectly, validating our proposed methods. We observe that the CT efficiency shows a transition across the A-exciton resonance of WS_2: Below it, the CT efficiency is relatively inefficient with a quantum yield of <1%; above it, the CT efficiency increases with the increasing excitation energy and reaches ~5% for 3.10-eV excitation. One of the origins for the much-enhanced CT efficiency in the DHT regime in comparison to that for the photo-thermionic emission regime could be attributed to the density of electrons in graphene for CT: In the photo-thermionic emission regime, only a limited number (on the order of 10^{11} to 10^{12} cm^{-2}) of electrons with sufficiently high energy can be emitted over the energy barrier, while in the DHT regime, the valence band electrons in graphene, with a much higher density (on the order of ~10^{14} cm^{-2}), can efficiently recombine with the photogenerated holes in the valence band of WS_2. Furthermore, in the DHT regime, we observe that DHT efficiency goes up with increasing the excitation photon energy ($h\nu$). This result can be rationalized by partial extraction of hot holes to graphene before cooling down to the A-exciton state in WS_2.

Our data here provide direct and strong evidence for the transition of the CT mechanism from HET (via photo-thermionic emission when only graphene is excited) to DHT between the valence bands from WS_2 to graphene (in the above-A-exciton excitation regime). Last, in the sub-A-exciton excitation regime, while it is clear that HET via photo-thermionic emission takes place ($\alpha_{THz\text{-}OPTP} > 1$ for $h\nu < 2.0$ eV), it remains ambiguous if other HET pathways are possible. To check this aspect, we renormalize the maximum positive photoconductivity to the incident power (*P*, rather than N_{abs} as shown in Fig. 3D) and replot it versus the pump photon energy. As the electron temperature in graphene is independent of the pump photon energy for a fixed incident power, the HET efficiency via pure photo-thermionic emission will be constant for different pump photon energies in such a plot (*27*, *28*). As shown in fig. S6, for $h\nu < 1$ eV, the HET efficiency is nearly constant, in line with photo-thermionic emission; for $1.4 < h\nu < 2$ eV, we observe an increase in the HET efficiency. This indicates that in the sub-A-exciton excitation regime, with sufficiently high pump photon energy, other possible CT routes may also contribute to the CT process. One of the plausible scenarios is CT involving nonthermalized hot electrons (on top of photo-thermionic emission). Knowing the energy difference between the WS_2 CBM and graphene's Dirac point (~0.7 eV), the minimum pump energy required for nonthermalized hot electron injection is 2×0.7 eV = 1.4 eV, in line with the experimental observation. However, further studies are needed to rule out other possible CT mechanisms, such as DHT at graphene and small domains of multilayer WS_2 (with absorption onset around 1.3 eV) (*21*).

DISCUSSION

We unveil new injection and recombination pathways in g-TMDCs and demonstrate the beneficial effect of interfacial defect states for

promoting a long interfacial charge separation time and thus an efficient photogating phenomenon in g-based vdW structures. Understanding such injection and recombination pathways is important for both fundamental studies and optoelectronic applications. For instance, the long-lived photogating effect reported here (mediated by ultrafast interfacial CT and interfacial trapping process) reconciles the reported very short charge separation time at g-TMDCs interfaces (*10*, *11*) and, however, very efficient photodetectors based on these structures (*5*–*7*). While interfacial defects are beneficial in such circumstance, their impact on the performance of other optoelectronic devices depends strongly on the application: for instance, high density of interfacial defects is troublesome for photovoltaics, where an efficient electron and hole separation toward electrodes is required for highly performed devices. The short lifetime of injected hot electrons in the conduction band of TMDCs imposes a limited time window for the efficient separation of charges toward electrodes. Passivation of the interfacial states or development of further extraction of injected hot electrons from TMDCs through an ultrafast, subpicosecond channel is required.

In summary, we investigate the nonequilibrium hot carrier dynamics in g-WS_2 vdW heterostructures combining ultrafast THz and TA spectroscopy. We report a transition in both CT efficiency and mechanism by tuning the pump photon energies across the A-exciton resonance of WS_2. Upon excitation below the A-exciton resonance of WS_2, a relatively inefficiently HET via photo-thermionic emission governs the CT process, and only thermalized hot electrons with sufficient energy can be injected into the excited states of WS_2. In contrast, we show that highly energetic nonthermalized hot electrons in graphene do not contribute to the CT process. Rather, a relatively efficient (up to ~5%) DHT process occurs from the valence band of WS_2 to the valence band of graphene. We show that the injected electrons only occupy the excited states of WS_2 for ~1 ps and then get trapped and stored at vdW interfaces (probed by TA spectroscopy). This results in a long-lived photogating effect in graphene over 1 ns (observed by THz spectroscopy). Our results here provide new insights into both the CT mechanism and recombination pathway at g-TMDCs vdW interfaces, which are critical to potential optoelectronic and energy-harvesting applications of g-TMDCs vdW heterostructures.

MATERIALS AND METHODS

Sample information

The g-WS_2 heterostructure on a sapphire substrate is obtained commercially (from SixCarbon Technology, Shenzhen) and produced by CVD method. The heterostructure is characterized by UV-vis spectroscopy, Raman spectroscopy, and THz-TDS to examine the number of layers and E_F in graphene.

OPTP spectroscopy

To track ultrafast charge flow across the g-WS_2 interfaces, we perform OPTP spectroscopy to study photoconductivity of the samples. The THz spectrometer is powered by a femtosecond laser (based on regenerative amplified and mode-locked Ti:sapphire) with a central wavelength of 800 nm, a pulse length of ~50 fs, and a repeating frequency of 1 kHz. For optical excitations, the fundamental wavelength (800 nm) and the frequency doubled wavelength (400 nm) by using a BiB_3O_6 crystal can be readily achieved; other wavelengths are obtained by a commercial optical parametric amplifier from Light Conversion. The THz electrical field in the time domain is mapped out by electro-optic sampling method.

SUPPLEMENTARY MATERIALS

Supplementary material for this article is available at http://advances.sciencemag.org/cgi/content/full/7/9/eabd9061/DC1

REFERENCE AND NOTES

1. Y. Liu, Y. Huang, X. Duan, Van der Waals integration before and beyond two-dimensional materials. *Nature* **567**, 323–333 (2019).
2. D. Jariwala, T. J. Marks, M. C. Hersam, Mixed-dimensional van der Waals heterostructures. *Nat. Mater.* **16**, 170–181 (2017).
3. K. S. Novoselov, A. Mishchenko, A. Carvalho, A. H. C. Neto, 2D materials and van der Waals heterostructures. *Science* **353**, aac9439 (2016).
4. A. K. Geim, I. V. Grigorieva, Van der Waals heterostructures. *Nature* **499**, 419–425 (2013).
5. F. H. L. Koppens, T. Mueller, P. Avouris, A. C. Ferrari, M. S. Vitiello, M. Polini, Photodetectors based on graphene, other two-dimensional materials and hybrid systems. *Nat. Nanotechnol.* **9**, 780–793 (2014).
6. M. Massicotte, P. Schmidt, F. Vialla, K. G. Schädler, A. Reserbat-Plantey, K. Watanabe, T. Taniguchi, K. J. Tielrooij, F. H. L. Koppens, Picosecond photoresponse in van der Waals heterostructures. *Nat. Nanotechnol.* **11**, 42–46 (2016).
7. J. Shim, D.-H. Kang, Y. Kim, H. Kum, W. Kong, S.-H. Bae, I. Almansouri, K. Lee, J.-H. Park, J. Kim, Recent progress in Van der Waals (vdW) heterojunction-based electronic and optoelectronic devices. *Carbon* **133**, 78–89 (2018).
8. W. Zhang, C.-P. Chuu, J.-K. Huang, C.-H. Chen, M.-L. Tsai, Y.-H. Chang, C.-T. Liang, Y.-Z. Chen, Y.-L. Chueh, J.-H. He, Ultrahigh-gain photodetectors based on atomically thin graphene-MoS_2 heterostructures. *Sci. Rep.* **4**, 3826 (2014).
9. G. Konstantatos, M. Badioli, L. Gaudreau, J. Osmond, M. Bernechea, F. P. G. De Arquer, F. Gatti, F. H. L. Koppens, Hybrid graphene–quantum dot phototransistors with ultrahigh gain. *Nat. Nanotechnol.* **7**, 363–368 (2012).
10. Y. Chen, Y. Li, Y. Zhao, H. Zhou, H. Zhu, Highly efficient hot electron harvesting from graphene before electron-hole thermalization. *Sci. Adv.* **5**, eaax9958 (2019).
11. L. Yuan, T. F. Chung, A. Kuc, Y. Wan, Y. Xu, Y. P. Chen, T. Heine, L. Huang, Photocarrier generation from interlayer charge-transfer transitions in WS_2-graphene heterostructures. *Sci. Adv.* **4**, e1700324 (2018).
12. S. Aeschlimann, A. Rossi, M. Chávez-Cervantes, R. Krause, B. Arnoldi, B. Stadtmüller, M. Aeschlimann, S. Forti, F. Fabbri, C. Coletti, Direct evidence for efficient ultrafast charge separation in epitaxial WS_2/graphene heterostructures. *Sci. Adv.* **6**, eaay0761 (2020).
13. A. Rose, *Concepts in Photoconductivity and Allied Problems* (Interscience publishers, 1963).
14. J. D. Mehew, S. Unal, E. Torres Alonso, G. F. Jones, S. Fadhil Ramadhan, M. F. Craciun, S. Russo, Fast and highly sensitive ionic-polymer-gated WS_2–graphene photodetectors. *Adv. Mater.* **29**, 1700222 (2017).
15. T. Chen, Y. Sheng, Y. Zhou, R. Chang, X. Wang, H. Huang, Q. Zhang, L. Hou, J. H. Warner, High photoresponsivity in ultrathin 2D lateral graphene: WS_2: Graphene photodetectors using direct CVD growth. *ACS Appl. Mater. Interfaces* **11**, 6421–6430 (2019).
16. M. Breusing, S. Kuehn, T. Winzer, E. Malić, F. Milde, N. Severin, J. P. Rabe, C. Ropers, A. Knorr, T. Elsaesser, Ultrafast nonequilibrium carrier dynamics in a single graphene layer. *Phys. Rev. B.* **83**, 153410 (2011).
17. D. Brida, A. Tomadin, C. Manzoni, Y. J. Kim, A. Lombardo, S. Milana, R. R. Nair, K. S. Novoselov, A. C. Ferrari, G. Cerullo, Ultrafast collinear scattering and carrier multiplication in graphene. *Nat. Commun.* **4**, 1987 (2013).
18. K. J. Tielrooij, L. Piatkowski, M. Massicotte, A. Woessner, Q. Ma, Y. Lee, K. S. Myhro, C. N. Lau, P. Jarillo-Herrero, N. F. Van Hulst, F. H. L. Koppens, Generation of photovoltage in graphene on a femtosecond timescale through efficient carrier heating. *Nat. Nanotechnol.* **10**, 437–443 (2015).
19. K. J. Tielrooij, J. C. W. Song, S. A. Jensen, A. Centeno, A. Pesquera, A. Zurutuza Elorza, M. Bonn, L. S. Levitov, F. H. L. Koppens, Photoexcitation cascade and multiple hot-carrier generation in graphene. *Nat. Phys.* **9**, 248–252 (2013).
20. I. Gierz, J. C. Petersen, M. Mitrano, C. Cacho, I. C. E. Turcu, E. Springate, A. Stöhr, A. Köhler, U. Starke, A. Cavalleri, Snapshots of non-equilibrium Dirac carrier distributions in graphene. *Nat. Mater.* **12**, 1119–1124 (2013).
21. Z. Mics, K.-J. Tielrooij, K. Parvez, S. A. Jensen, I. Ivanov, X. Feng, K. Müllen, M. Bonn, D. Turchinovich, Thermodynamic picture of ultrafast charge transport in graphene. *Nat. Commun.* **6**, 7655 (2015).
22. J. C. W. Song, M. Y. Reizer, L. S. Levitov, Disorder-assisted electron-phonon scattering and cooling pathways in graphene. *Phys. Rev. Lett.* **109**, 106602 (2012).
23. M. W. Graham, S. F. Shi, D. C. Ralph, J. Park, P. L. McEuen, Photocurrent measurements of supercollision cooling in graphene. *Nat. Phys.* **9**, 103–108 (2013).

24. A. C. Betz, S. H. Jhang, E. Pallecchi, R. Ferreira, G. Fève, J.-M. Berroir, B. Plaçais, Supercollision cooling in undoped graphene. *Nat. Phys.* **9**, 109–112 (2013).
25. M. T. Mihnev, F. Kadi, C. J. Divin, T. Winzer, S. Lee, C.-H. Liu, Z. Zhong, C. Berger, W. A. De Heer, E. Malic, Microscopic origins of the terahertz carrier relaxation and cooling dynamics in graphene. *Nat. Commun.* **7**, 11617 (2016).
26. T. Low, V. Perebeinos, R. Kim, M. Freitag, P. Avouris, Cooling of photoexcited carriers in graphene by internal and substrate phonons. *Phys. Rev. B.* **86**, 045413 (2012).
27. M. Massicotte, P. Schmidt, F. Vialla, K. Watanabe, T. Taniguchi, K. J. Tielrooij, F. H. L. Koppens, Photo-thermionic effect in vertical graphene heterostructures. *Nat. Commun.* **7**, 12174 (2016).
28. Q. Ma, T. I. Andersen, N. L. Nair, N. M. Gabor, M. Massicotte, C. H. Lui, A. F. Young, W. Fang, K. Watanabe, T. Taniguchi, J. Kong, N. Gedik, F. H. L. Koppens, P. Jarillo-Herrero, Tuning ultrafast electron thermalization pathways in a van der Waals heterostructure. *Nat. Phys.* **12**, 455–459 (2016).
29. Z. Y. Zhu, Y. C. Cheng, U. Schwingenschlögl, Giant spin-orbit-induced spin splitting in two-dimensional transition-metal dichalcogenide semiconductors. *Phys. Rev. B.* **84**, 153402 (2011).
30. B. Zhu, X. Chen, X. Cui, Exciton binding energy of monolayer WS_2. *Sci. Rep.* **5**, 9218 (2015).
31. H. M. Hill, A. F. Rigosi, A. Raja, A. Chernikov, C. Roquelet, T. F. Heinz, Exciton broadening in WS_2/graphene heterostructures. *Phys. Rev. B.* **96**, 205401 (2017).
32. R. R. Nair, P. Blake, A. N. Grigorenko, K. S. Novoselov, T. J. Booth, T. Stauber, N. M. R. Peres, A. K. Geim, Fine structure constant defines visual transparency of graphene. *Science* **320**, 1308 (2008).
33. K. F. Mak, M. Y. Sfeir, Y. Wu, C. H. Lui, J. A. Misewich, T. F. Heinz, Measurement of the optical conductivity of graphene. *Phys. Rev. Lett.* **101**, 196405 (2008).
34. R. Ulbricht, E. Hendry, J. Shan, T. F. Heinz, M. Bonn, Carrier dynamics in semiconductors studied with time-resolved terahertz spectroscopy. *Rev. Mod. Phys.* **83**, 543–586 (2011).
35. S.-F. Shi, T.-T. Tang, B. Zeng, L. Ju, Q. Zhou, A. Zettl, F. Wang, Controlling graphene ultrafast hot carrier response from metal-like to semiconductor-like by electrostatic gating. *Nano Lett.* **14**, 1578–1582 (2014).
36. S. A. Jensen, Z. Mics, I. Ivanov, H. S. Varol, D. Turchinovich, F. H. L. Koppens, M. Bonn, K.-J. Tielrooij, Competing ultrafast energy relaxation pathways in photoexcited graphene. *Nano Lett.* **14**, 5839–5845 (2014).
37. A. J. Frenzel, C. H. Lui, Y. C. Shin, J. Kong, N. Gedik, Semiconducting-to-metallic photoconductivity crossover and temperature-dependent Drude weight in graphene. *Phys. Rev. Lett.* **113**, 56602 (2014).
38. A. Tomadin, S. M. Hornett, H. I. Wang, E. M. Alexeev, A. Candini, C. Coletti, D. Turchinovich, M. Kläui, M. Bonn, F. H. L. Koppens, E. Hendry, M. Polini, K.-J. Tielrooij, The ultrafast dynamics and conductivity of photoexcited graphene at different Fermi energies. *Sci. Adv.* **4**, eaar5313 (2018).
39. H. I. Wang, M.-L. Braatz, N. Richter, K.-J. Tielrooij, Z. Mics, H. Lu, N.-E. Weber, K. Müllen, D. Turchinovich, M. Kläui, M. Bonn, Reversible photochemical control of doping levels in supported graphene. *J. Phys. Chem. C* **121**, 4083–4091 (2017).
40. G. Jnawali, Y. Rao, H. Yan, T. F. Heinz, Observation of a transient decrease in terahertz conductivity of single-layer graphene induced by ultrafast optical excitation. *Nano Lett.* **13**, 524–530 (2013).
41. S. L. Palfrey, T. F. Heinz, Coherent interactions in pump–probe absorption measurements: The effect of phase gratings. *JOSA B.* **2**, 674–679 (1985).
42. G. Grimaldi, R. W. Crisp, S. Ten Brinck, F. Zapata, M. Van Ouwendorp, N. Renaud, N. Kirkwood, W. H. Evers, S. Kinge, I. Infante, L. D. A. Siebbeles, A. J. Houtepen, Hot-electron transfer in quantum-dot heterojunction films. *Nat. Commun.* **9**, 2310 (2018).
43. H. Wang, C. Zhang, F. Rana, Ultrafast dynamics of defect-assisted electron–hole recombination in monolayer MoS_2. *Nano Lett.* **15**, 339–345 (2015).
44. P. D. Cunningham, K. M. McCreary, A. T. Hanbicki, M. Currie, B. T. Jonker, L. M. Hayden, Charge trapping and exciton dynamics in large-area CVD grown MoS_2. *J. Phys. Chem. C* **120**, 5819–5826 (2016).
45. C. J. Docherty, P. Parkinson, H. J. Joyce, M.-H. Chiu, C.-H. Chen, M.-Y. Lee, L.-J. Li, L. M. Herz, M. B. Johnston, Ultrafast transient terahertz conductivity of monolayer MoS_2 and WSe_2 grown by chemical vapor deposition. *ACS Nano* **8**, 11147–11153 (2014).
46. H. Wang, C. Zhang, F. Rana, Surface recombination limited lifetimes of photoexcited carriers in few-layer transition metal dichalcogenide MoS_2. *Nano Lett.* **15**, 8204–8210 (2015).
47. B. Schuler, D. Y. Qiu, S. Refaely-Abramson, C. Kastl, C. T. Chen, S. Barja, R. J. Koch, D. F. Ogletree, S. Aloni, A. M. Schwartzberg, Large spin-orbit splitting of deep in-gap defect states of engineered sulfur vacancies in monolayer WS_2. *Phys. Rev. Lett.* **123**, 76801 (2019).
48. M. R. Rosenberger, H.-J. Chuang, K. M. McCreary, C. H. Li, B. T. Jonker, Electrical characterization of discrete defects and impact of defect density on photoluminescence in monolayer WS_2. *ACS Nano* **12**, 1793–1800 (2018).
49. J. Hong, Z. Hu, M. Probert, K. Li, D. Lv, X. Yang, L. Gu, N. Mao, Q. Feng, L. Xie, Exploring atomic defects in molybdenum disulphide monolayers. *Nat. Commun.* **6**, 6293 (2015).
50. S. C. Boehme, H. Wang, L. D. A. Siebbeles, D. Vanmaekelbergh, A. J. Houtepen, Electrochemical charging of CdSe quantum dot films: Dependence on void size and counterion proximity. *ACS Nano* **7**, 2500–2508 (2013).
51. S. C. Boehme, J. M. Azpiroz, Y. V. Aulin, F. C. Grozema, D. Vanmaekelbergh, L. D. A. Siebbeles, I. Infante, A. J. Houtepen, Density of trap states and Auger-mediated electron trapping in CdTe quantum-dot solids. *Nano Lett.* **15**, 3056–3066 (2015).
52. S. C. Boehme, T. A. Walvis, I. Infante, F. C. Grozema, D. Vanmaekelbergh, L. D. A. Siebbeles, A. J. Houtepen, Electrochemical control over photoinduced electron transfer and trapping in CdSe-CdTe quantum-dot solids. *ACS Nano* **8**, 7067–7077 (2014).
53. A. Raja, A. Chaves, J. Yu, G. Arefe, H. M. Hill, A. F. Rigosi, T. C. Berkelbach, P. Nagler, C. Schüller, T. Korn, C. Nuckolls, J. Hone, L. E. Brus, T. F. Heinz, D. R. Reichman, A. Chernikov, Coulomb engineering of the bandgap and excitons in two-dimensional materials. *Nat. Commun.* **8**, 15251 (2017).
54. D. Sun, Y. Rao, G. A. Reider, G. Chen, Y. You, L. Brézin, A. R. Harutyunyan, T. F. Heinz, Observation of rapid exciton–exciton annihilation in monolayer molybdenum disulfide. *Nano Lett.* **14**, 5625–5629 (2014).
55. E. del Corro, A. Botello-Méndez, Y. Gillet, A. L. Elias, H. Terrones, S. Feng, C. Fantini, D. Rhodes, N. Pradhan, L. Balicas, X. Gonze, J.-C. Charlier, M. Terrones, M. A. Pimenta, Atypical exciton–phonon interactions in WS_2 and WSe_2 monolayers revealed by resonance Raman spectroscopy. *Nano Lett.* **16**, 2363–2368 (2016).
56. J. Yan, Y. Zhang, P. Kim, A. Pinczuk, Electric field effect tuning of electron-phonon coupling in graphene. *Phys. Rev. Lett.* **98**, 166802 (2007).
57. A. Das, S. Pisana, B. Chakraborty, S. Piscanec, S. K. Saha, U. V. Waghmare, K. S. Novoselov, H. R. Krishnamurthy, A. K. Geim, A. C. Ferrari, A. K. Sood, Monitoring dopants by Raman scattering in an electrochemically top-gated graphene transistor. *Nat. Nanotechnol.* **3**, 210–215 (2008).
58. M. Tinkham, Energy gap interpretation of experiments on infrared transmission through superconducting films. *Phys. Rev.* **104**, 845–846 (1956).
59. S. H. Abedinpour, G. Vignale, A. Principi, M. Polini, W. K. Tse, A. H. Macdonald, Drude weight, plasmon dispersion, and ac conductivity in doped graphene sheets. *Phys. Rev. B.* **84**, 045429 (2011).
60. J. Horng, C. F. Chen, B. Geng, C. Girit, Y. Zhang, Z. Hao, H. A. Bechtel, M. Martin, A. Zettl, M. F. Crommie, Y. R. Shen, F. Wang, Drude conductivity of Dirac fermions in graphene. *Phys. Rev. B.* **83**, 165113 (2011).
61. E. H. Hwang, S. Adam, S. Das Sarma, Carrier transport in two-dimensional graphene layers. *Phys. Rev. Lett.* **98**, 186806 (2007).
62. H. Henck, Z. B. Aziza, D. Pierucci, F. Laourine, F. Reale, P. Palczynski, J. Chaste, M. G. Silly, F. Bertran, P. L. Fèvre, E. Lhuillier, T. Wakamura, C. Mattevi, J. E. Rault, M. Calandra, A. Ouerghi, Electronic band structure of two-dimensional WS_2/graphene van der Waals heterostructures. *Phys. Rev. B.* **97**, 155421 (2018).
63. A. Ramasubramaniam, Large excitonic effects in monolayers of molybdenum and tungsten dichalcogenides. *Phys. Rev. B.* **86**, 115409 (2012).
64. S. Das, H.-Y. Chen, A. V. Penumatcha, J. Appenzeller, High performance multilayer MoS_2 transistors with scandium contacts. *Nano Lett.* **13**, 100–105 (2013).
65. Y. Liu, P. Stradins, S.-H. Wei, Van der Waals metal-semiconductor junction: Weak Fermi level pinning enables effective tuning of Schottky barrier. *Sci. Adv.* **2**, e1600069 (2016).
66. T. Le Quang, V. Cherkez, K. Nogajewski, M. Potemski, M. T. Dau, M. Jamet, P. Mallet, J.-Y. Veuillen, Scanning tunneling spectroscopy of van der Waals graphene/semiconductor interfaces: Absence of Fermi level pinning. *2D Mater.* **4**, 35019 (2017).
67. K. I. Bolotin, K. J. Sikes, Z. Jiang, M. Klima, G. Fudenberg, J. Hone, P. Kim, H. L. Stormer, Ultrahigh electron mobility in suspended graphene. *Solid State Commun.* **146**, 351–355 (2008).
68. W. Norimatsu, M. Kusunoki, Epitaxial graphene on SiC {0001}: Advances and perspectives. *Phys. Chem. Chem. Phys.* **16**, 3501–3511 (2014).
69. L. Banszerus, M. Schmitz, S. Engels, J. Dauber, M. Oellers, F. Haupt, K. Watanabe, T. Taniguchi, B. Beschoten, C. Stampfer, Ultrahigh-mobility graphene devices from chemical vapor deposition on reusable copper. *Sci. Adv.* **1**, e1500222 (2015).

Acknowledgments: We thank P. Soltani, A. S. Hassan, Z. Liu, M. Ballabio, A. Tries, K. Krewer, B. Kutus, and M. Kläui for the fruitful discussions. **Funding:** S.F. acknowledges fellowship support from Chinese Scholarship Council (CSC). X.J. acknowledges financial support by DFG through the Excellence Initiative by the Graduate School of Excellence Materials Science in Mainz (MAINZ) (GSC 266) and support from the Max Planck Graduate Center mit der Johannes Gutenberg-Universität Mainz (MPGC). A.J.H. acknowledges support from the European Research Council Horizon 2020 ERC grant no. 678004 (Doping on Demand). ICN2 was supported by the Severo Ochoa program from Spanish MINECO (grant no. SEV-2017-0706). K.-J.T. acknowledges funding from the European Union's Horizon 2020 Research and Innovation Programme under grant agreement no. 804349 (ERC StG CUHL) and financial

support through the MAINZ Visiting Professorship. **Author contributions:** H.I.W. conceived and supervised the project. S.F. conducted THz studies, with help from X.J., J.X., X.Y., H.Z., W.Z., and S.K. I.d.F. conducted TA measurements and analyzed the data under the supervision of A.J.H. X.J. and K.-J.T. modeled the electron temperature in graphene based on THz conductivity. All authors contributed to data interpretation. S.F. and H.I.W. wrote the paper with input from all authors. **Competing interests:** The authors declare that they have no competing interests. **Data and materials availability:** All data needed to evaluate the conclusions in the paper are present in the paper and/or the Supplementary Materials. Additional data related to this paper may be requested from the authors.

Submitted 20 July 2020
Accepted 12 January 2021
Published 26 February 2021
10.1126/sciadv.abd9061

Citation: S. Fu, I. du Fossé, X. Jia, J. Xu, X. Yu, H. Zhang, W. Zheng, S. Krasel, Z. Chen, Z. M. Wang, K.-J. Tielrooij, M. Bonn, A. J. Houtepen, H. I. Wang, Long-lived charge separation following pump-wavelength–dependent ultrafast charge transfer in graphene/WS_2 heterostructures. *Sci. Adv.* **7**, eabd9061 (2021).

Science Advances

Long-lived charge separation following pump-wavelength–dependent ultrafast charge transfer in graphene/WS_2 heterostructures

Shuai Fu, Indy du Fossé, Xiaoyu Jia, Jingyin Xu, Xiaoqing Yu, Heng Zhang, Wenhao Zheng, Sven Krasel, Zongping Chen, Zhiming M. Wang, Klaas-Jan Tielrooij, Mischa Bonn, Arjan J. Houtepen and Hai I. Wang

Sci Adv **7** (9), eabd9061.
DOI: 10.1126/sciadv.abd9061